JGR Planets

RESEARCH ARTICLE
10.1029/2021JE006976

Key Points:

- In equinoxes, helium bulges are observed to extend from mid-latitudes in to the southern polar regions (>60°S)
- The observed helium densities in the southern polar regions in equinoxes are 10–30 × greater than the modeled ones
- The observed winds seem to support the formation of helium bulge in the southern polar region during the autumnal equinox

Correspondence to:
N. V. Rao,
nvrao@narl.gov.in

Citation:
Gupta, N., Rao, N. V., Bougher, S., & Elrod, M. K. (2021). Latitudinal and seasonal asymmetries of the helium bulge in the Martian upper atmosphere. *Journal of Geophysical Research: Planets*, *126*, e2021JE006976. https://doi.org/10.1029/2021JE006976

Received 10 JUN 2021
Accepted 1 SEP 2021

Latitudinal and Seasonal Asymmetries of the Helium Bulge in the Martian Upper Atmosphere

Neha Gupta[1], N. V. Rao[1], S. Bougher[2], and M. K. Elrod[3,4]

[1]National Atmospheric Research Laboratory, Gadanki, India, [2]Department of Climate and Space Sciences and Engineering, University of Michigan, Ann Arbor, MI, USA, [3]NASA Goddard Space Flight Center, Greenbelt, MD, USA, [4]CRESST University of Maryland College Park, College Park, MD, USA

Abstract In the present study, we investigate the characteristics of helium (He) bulges in the Martian upper atmosphere using He densities and winds measured by the Neutral Gas and Ion Mass Spectrometer (NGIMS) aboard the Mars Atmosphere and Volatile EvolutioN (MAVEN) spacecraft. The observations are compared with those predicted by the Mars Global Ionosphere Thermosphere Model (M-GITM). The results of the present study show that the nightside He bulge is a persistent feature of the Martian upper atmosphere in all seasons. The He densities inside the bulges are 1–2 orders of magnitude greater than those on the dayside. In solstices, the bulges are observed in the winter polar region which is in accordance with the model predictions. In equinoxes, however, the bulges are observed to extend from mid-latitudes into the southern polar regions (>60°S), which is contrary to the model predictions at mid-latitudes. These anomalous bulges are predominantly observed in the northern spring equinox and are 10–30 × greater than the modeled ones. During the autumnal equinox, the observed winds depart from the modeled winds. Furthermore, the observed winds point to the southern polar regions where the bulges are observed. Thus, the results of the present study indicate that in equinoxes the regions of local vertical advection, that are responsible for the formation of the bulges, are displaced toward the southern polar regions. The results of the present study point to the need of a larger wind database from NGIMS in southern polar region, particularly during equinoxes.

Plain Language Summary Helium in the upper atmospheres of Earth, Venus, and Mars is known to accumulate on the nightside which is often referred as "He bulge." The upwelling of winds on the dayside and their downwelling on the nightside, combined with large-scale circulation, is the primary driver of the bulge formation. The densities inside the He bulge are, in general, 1–2 orders of magnitude greater than those on the dayside. In the present study, the He bulge in the Mars upper atmosphere is investigated using the neutral densities measured by the Mars Atmosphere and Volatile EvolutioN spacecraft and those of a global model. In the northern summer, the He bulge occurs in the winter polar nightside which is in accordance with the model predictions. In spring and autumn, however, the observed He bulges extend from mid-latitudes into the southern polar region whereas the model predicts their presence at mid-latitudes. The southern polar bulges in autumn are observed in regions where the observed winds point toward the southern pole. Inclusion of the effects of the upward propagating small-scale waves on the Martian upper atmosphere in the model, along with a larger observational wind database, is likely to address the data-model differences.

1. Introduction

The Mars thermosphere extends from the top of the mesopause (~100 km) to the exobase (~220 km) and its composition is dominated by CO_2 with O, O_2, Ar, N_2, CO, NO, C, He, and N being the other important neutral species (e.g., Bougher, Jakosky, et al., 2015). O becomes the dominant neutral species above somewhere between 180 and 270 km in the upper thermosphere and exosphere (e.g., Bhardwaj et al., 2016; Bougher, Jakosky, et al., 2015; Mahaffy et al., 2015; Venkateswara Rao et al., 2020). The basic thermal structure of the Martian thermosphere is well established by several measurements from the Viking landers to those currently from the Mars Atmosphere and Volatile Evolution (MAVEN) mission (Bougher et al., 2017; Bougher, Cravens et al., 2015; Stone et al., 2018 and references therein). While the absorption of solar X-ray and EUV radiation heats the Martian thermosphere, thermal conduction and 15-μm CO_2 radiative cooling act as major sinks to the heat. On the nightside, solar heating is absent but the cooling processes still operate.

This results in day-to-night temperature gradient and hence dayside expansion and nightside contraction of the Martian thermosphere (e.g., Gupta et al., 2019; Stone et al., 2018). Furthermore, differential heating between the summer and winter hemispheres also leads to upwelling in the summer hemisphere and downwelling in the winter hemisphere thereby leading to summer to winter meridional circulation in the thermosphere. Global circulation models (GCMs), such as the Mars Global Ionosphere Thermosphere Model (M-GITM) and Laboratoire de Météorologie Dynamique Mars GCM (LMD-MGCM), are able to capture this basic structure of the Martian upper atmosphere reasonably well (Bougher, Pawlowski, et al., 2015; González-Galindo et al., 2015).

In addition to heating and cooling, persistent forcing by gravity waves (England et al., 2017; Fritts et al., 2006; Mahaffy et al., 2015; Medvedev & Yiğit, 2012; Terada et al., 2017; Williamson et al., 2019), thermal tides (Lee et al., 2009; Liu et al., 2017; Wilson, 2002), planetary waves (Hinson et al., 2003; Moudden & Forbes, 2010), seasonal inflation and contraction of the lower atmosphere (e.g., Bougher, Pawlowski, et al., 2015) and episodic forcings such as planet-encircling dust events (Elrod et al., 2020; Jain et al., 2020; Kuroda et al., 2020; Leelavathi et al., 2020; Liu et al., 2018; Venkateswara Rao et al., 2020) also play a key role in the energy redistribution and compositional changes in the Mars upper atmosphere. These forcings are indicative of energy transfer from the lower atmosphere to the thermosphere and hence coupling between the two regions (e.g., Bougher, Cravens et al., 2015). Occasional heating of the thermosphere by solar flares (Thiemann et al., 2015, 2018) further complicates the temporal and seasonal variability of the Mars thermosphere.

Thermospheric composition shows species dependent response to thermal and dynamical forcings. Heavier species (such as CO_2 and Ar), due to their small scale-height, show stronger response to changes in the heating than the lighter species (Bougher, Pawlowski, et al., 2015). Since CO_2 is the dominant neutral species, the thermosphere expands in regions of heating and contracts in regions of cooling. The lighter species (such as He and O), on the other hand, respond more to the background circulation (zonal and meridional winds) and related vertical advection (upwelling and downwelling) leading to their accumulation at specific locations and local times (Bougher et al., 2008; Bougher, Pawlowski, et al., 2015; Cageao & Kerr, 1984; Johnson & Gottlieb, 1970; Liu et al., 2014; Reber & Hays, 1973). Therefore, He/CO_2 ratio is often used to better appreciate the He bulge in the Martian thermosphere (e.g., Elrod et al., 2017). Liu et al. (2014) have shown that while the vertical advection and molecular diffusion are the dominant processes for the formation of He bulge on Earth, horizontal winds contribute indirectly by maintaining the thermospheric mass continuity. A similar process is envisaged to operate on Mars as well for the formation of the He bulge (Bougher, Pawlowski, et al., 2015; Elrod et al., 2017). Accordingly, the upwelling part of the vertical advection on the dayside leads to the depreciation of lighter species (i.e., the He/CO_2 ratio decreases). The meridional winds propagate poleward on the dayside which after crossing poles converge on the nightside. The downwelling of winds at the convergent point leads to the accumulation of lighter species (particularly helium, where He/CO_2 ratio increases) and formation of a bulge on the nightside (Bougher, Pawlowski, et al., 2015; Elrod et al., 2017). Zonal winds cause local time variations of the bulge by moving the downwelling part of the vertical advection toward morning and evening terminators. This nightside convergence point also moves latitudinally with season. During equinoxes the convergent points lie in the mid-latitudes whereas in solstices the convergence happens in the winter polar regions. Modeling studies also predicted formation of the bulges in the Martian thermosphere (Bougher, Pawlowski, et al., 2015; Elrod et al., 2017).

The He bulge, in general, is referred to as the winter He bulge wherein the He densities in the winter polar region are 1–2 orders of magnitude higher than those in the summer polar region. Existence of such a winter bulge has been well reported for Earth (Kasprzak, 1969; Keating & Prior, 1968; Liu et al., 2014; Mauersberger et al., 1976; Reber et al., 1968; Thayer et al., 2012) and Venus (Kasprzak et al., 1993; Krasnopolsky & Gladstone, 2005; Niemann et al., 1980). Prior to MAVEN, the He observations on Mars were only those measured by the Extreme Ultraviolet Explorer Satellite in airglow remote sensing method (Krasnopolsky et al., 1994). Using the He measurements by the Neutral Gas and Ion Mass Spectrometer (NGIMS) onboard MAVEN, Elrod et al. (2017) reported the existence of the He bulges in the winter polar nightside. They found that the He abundance in the northern polar winter nightside is twice that on the northern polar summer nightside. The nightside enhancements in density are a factor of 10–20 larger than the dayside depreciations. These initial observations were found to agree preliminarily with the MGITM modeling results (Elrod et al., 2017).

The present study finds its importance in three major contexts. First, since the initial report of He bulge on Mars by Elrod et al. (2017), there has been a substantial amount of He data collected by MAVEN that covers a wide range of latitudes, local times, and seasons. Due to the limited data set, Elrod et al. (2017) could not establish the presence of He bulge in the southern polar winter and also could not clearly resolve the seasonal and local time variations. The present study addresses these issues with the larger data set. Second, NGIMS/MAVEN has been measuring the altitude profiles of horizontal winds in the Martian thermosphere since 2016 (Benna et al., 2019; Roeten et al., 2019). These wind measurements span a range of local times and seasons and are useful to infer the actual circulation pattern of the Martian thermosphere. Such direct wind measurements are expected to be useful in understanding the transport of lighter species. Third, since the work of Elrod et al. (2017), there has been considerable improvement in the M-GITM code which needs to be validated with the observed He densities and winds (see Section 2.3 for more details). Considering these developments, we revisit the He bulge to get better insight on its spatial and temporal variability and to offer a more realistic explanation for its formation based on the improved M-GITM and direct wind measurements.

2. Observations and Model Simulations

2.1. NGIMS Density Measurements

MAVEN, with its suite of nine experiments, has been exploring the Martian upper atmosphere since September 2014. It is in a highly elliptical orbit with nominal periapsis and apoapsis altitudes of ~150 and ~6,200 km, respectively and an orbital period of ~4.5 hr (Since April 2019 the apoapsis is at ~4,400 km with a period of ~3.6 hr). Being in a highly inclined orbit (75°), it covers a range of latitudes in each of its periapsis passes. Each periapsis pass of MAVEN slowly precesses in local time and takes several months to complete one diurnal cycle at a given altitude.

NGIMS is one of the nine experiments onboard the MAVEN spacecraft (Mahaffy et al., 2014). It is a dual source in-situ quadrupole mass spectrometer, designed to measure abundances of neutrals and ions in the range of 2–150 amu in the Martian upper atmosphere. In each neutral species measurement, atmospheric gas first passes through the ionization region and subsequently through mass separation and detection regions to get the abundances of important neutral species. NGIMS operations are carried out by alternating between a closed and an open source to collect and sample atmospheric species (Benna & Elrod, 2019; Mahaffy et al., 2014). In the closed source mode, surface nonreactive species such as Ar, He, CO_2, N_2, and CO are measured and this mode of operation is carried out on every orbit. The open source mode, on the other hand, is used alternatively to measure the reactive neutral species and ions. For the present study, we use the He and CO_2 abundances measured in the closed source mode. Data retrieval procedures that are used to extract densities are detailed in Benna and Elrod (2019). In its nominal orbit, NGIMS measures atmospheric abundance between periapsis and up to an altitude of 500 km. During week-long deep dip campaigns, however, MAVEN's orbit is lowered to altitudes as low as ~120 km. Furthermore, between April 14, 2018 and November 12, 2018, NGIMS performed 19 campaigns dedicated to Ar measurements up to 1,200 km enabling characterization of the exospheric region (Leblanc et al., 2019). In the present study, however, we use NGIMS measurements of He and CO_2 densities between 160 and 300 km only.

2.2. NGIMS Observations of Horizontal Winds

During normal science operations, NGIMS measures the densities of neutral and ion species by maintaining its field of view (FOV) within ±2° of spacecraft's ram direction (Mahaffy et al., 2014, 2015). Since NGIMS is mounted on a movable Articulated Payload Platform (APP), its boresight can be changed by moving APP off the ram axis. This provided an opportunity to perform horizontal neutral wind measurements and thus wind mode was introduced to the instrument's operations since 2016 (Benna et al., 2019). In this new mode, APP is moved ±8° off the ram axis in local vertical and local horizontal planes, which enables NGIMS to measure direct along-track and across-track winds in the Martian upper atmosphere (Benna et al., 2019). During the wind mode of operation, NGIMS normal science operations (measurement of abundances) are paused and modulations in CO_2 abundance alone are measured. Each wind campaign lasts for 2–3 days and the subsequent campaigns are separated by one to several months. During each campaign NGIMS collects

wind measurements in a 5–10 set of MAVEN orbits that correspond to nearly the same sets of local time, latitude and altitudes. The winds are generally measured between ~140 and ~240 km with a ~30 s cadence. The magnitude of winds can vary by ±20 and ±6 m/s along and across MAVEN track respectively, owing to errors in data retrieval processes. Further details about the campaigns and the wind extraction procedure can be found in Benna et al. (2019).

The present study uses the Level 2, version 08, revision 01 density data of NGIMS database. We use the density measurements from all inbound periapsis passes starting from the Martian year (MY) 32 (solar longitude, Ls = 288°; February 11, 2015) until Ls = 230° in MY 35 (June 30, 2020). Due to instrumentation effects as mentioned in Elrod et al. (2017), we did not include the density data prior to February 15, 2015. For wind observations, we used v06_r01 data sets of Level 3 data products from 41 campaigns that span the period from 2016 to 2020. The winds measured during both the inbound and outbound segments are used. The winds from each campaign are averaged with a similar procedure as that of Roeten et al. (2019). The observed and modeled densities used in the present study are averaged over 5 km × 5° × 0.33 hr altitude-latitude-local solar time (LST) grids. In the present study, we have not included observations from Ls = 180° to Ls = 360° in MY 34 as there was a planet-encircling dust event (PEDE-2018) during this period and the focus of the present paper is to study the He bulges during nominal dust conditions. The variation of He densities during the PEDE-2018 will be dealt in a pending publication.

2.3. M-GITM Model

M-GITM is essentially a modified version of the terrestrial GITM to fit with the Martian environment using the Mars fundamental physical processes. M-GITM incorporates the key radiative processes and contains prognostic equations for ion-neutral chemistry of the Mars upper atmosphere. The modern M-GITM is a whole atmospheric model that can simulate the thermal, compositional, and dynamical structure of the Mars atmosphere from the ground to ~250 km. The model has 5 × 5° horizontal resolution and 2.5 km vertical resolution, and is normally run at 2-s time steps. Model physics and simulated features of the upper atmosphere (above ~80 km) are stressed in most applications of the M-GITM model thus far.

Unlike the Earth GITM code, the new M-GITM code currently simulates the conditions of the Martian atmosphere all the way to the surface (Bougher, Pawlowski et al., 2015). For the Mars lower atmosphere (~0–80 km), a state-of-the-art correlated-k radiation code was adapted from the NASA Ames Mars General Circulation Model (MGCM) (Haberle et al., 1999) for incorporation into M-GITM. This provides solar heating (long and short wavelength), seasonally variable aerosol heating, and CO_2 15-μm cooling in the local thermal equilibrium (LTE) region of the Mars atmosphere (below ~80 km). In addition, dust opacity distributions are typically prescribed based upon empirical dust opacity maps obtained from several Martian years of measurements (e.g., Montabone et al., 2015; Smith, 2004, 2009). For the Mars upper atmosphere (~80–250 km), a modern CO_2 Non Local thermodynamic equilibrium (NLTE) 15-μm cooling scheme has recently been implemented (e.g., Gonzalez-Galindo et al., 2013), along with MAVEN Extreme Ultraviolet Monitor (EUVM) L3 solar EUV and UV fluxes taken from the Flare Irradiance Spectral Model for Mars (FISM-M) empirical model outputs on a daily cadence (Thiemann et al., 2017). Subsequently, M-GITM thermospheric heating, dissociation and ionization rates are simulated at each time step (e.g., Bougher, Pawlowski, et al., 2015). Corresponding prognostic fields for neutral temperatures, neutral densities (CO_2, CO, N_2, O, O_2, He, Ar, and N^4S), and photochemical ion densities (CO_2^+, O_2^+, O^+, NO^+, and N_2^+), plus 3-component neutral winds are computed on a three-dimensional regular grid. For application in this paper, FISM-M fluxes are used for driving new M-GITM simulations for the four-cardinal seasons spanning MY33 (Ls = 0°, 90°, 180°, and 270°).

On several occasions, a suite of M-GITM simulations have been compared successfully with MAVEN NGIMS, IUVS, and Accelerometer measurements (e.g., Bougher et al., 2017; Bougher, Pawlowski, et al., 2015; Elrod et al., 2017; Pilinski et al., 2018; Zurek et al., 2017). Both remote and in-situ measurements are included in this extensive set of data-model comparisons and model validation studies. Data-model comparisons generally reveal that: (a) the M-GITM code well captures the basic dayside density variations of key neutral species and (b) M-GITM temperatures also closely match NGIMS and IUVS derived temperatures at low solar zenith angles (SZA). Furthermore, initial helium density distributions from early NGIMS data sets (Elrod et al., 2017) are compared to M-GITM predictions at 180 km. Even with limited data sampling, the

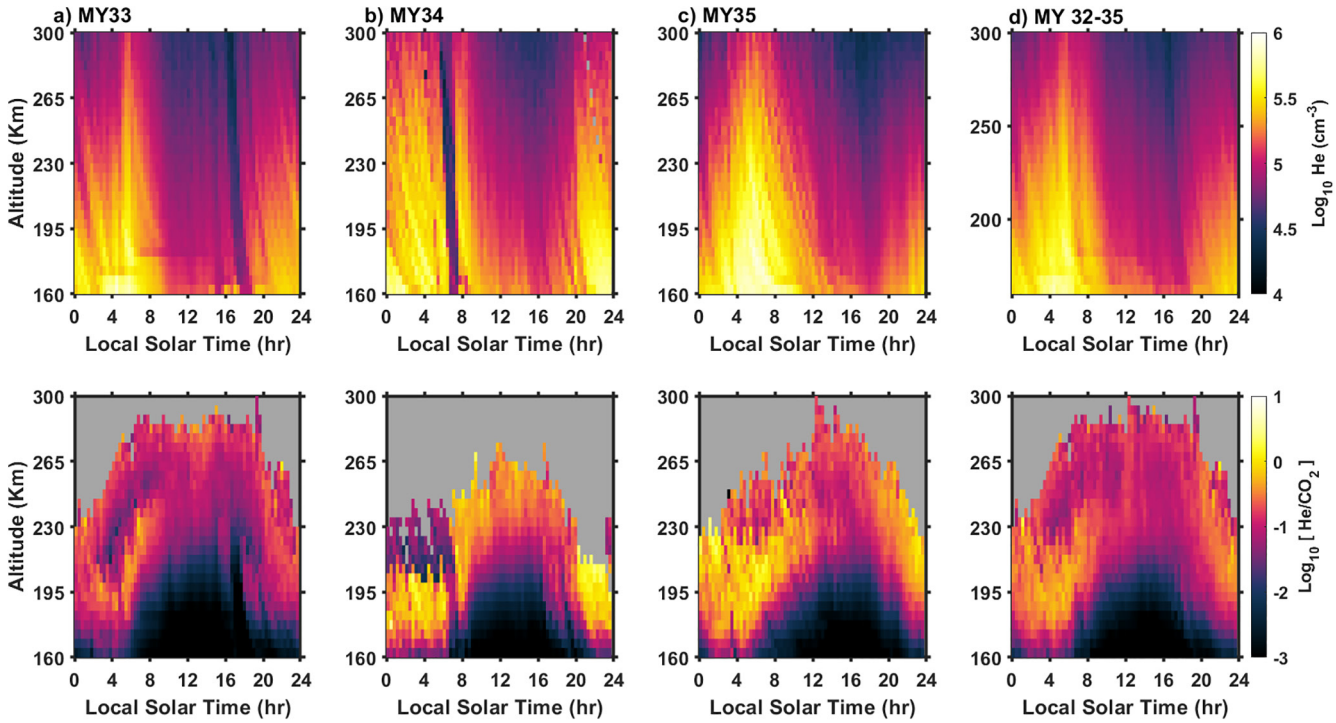

Figure 1. Local Solar Time (LST) versus altitude variability of (top panels) He densities and (bottom panels) He/CO_2 ratios during (a) MY 33, (b) MY 34, (c) MY 35, and (d) Average of MY 32–35. The data are averaged within an altitude and local time grid of 5 km × 0.33 hr.

basic observed features are simulated with significant helium bulges on the nightside. Nevertheless, Zurek et al. (2017) have reported that M-GITM versus MAVEN ACC mass density comparisons can be quite good from noon to the dusk terminator, but are poor from midnight toward the dawn terminator. The latter is likely due to incomplete M-GITM physics addressing gravity wave processes impacting global winds and the thermospheric circulation patterns throughout all seasons.

3. Results

The top panels of Figure 1 show the altitude versus local solar time (LST) variability of He densities. Note that as the data for MY 32 do not cover all LSTs, we do not show it separately but include it in Figure 1d. The patchiness in the data is mainly related to the data coverage. The low-density streaks observed at 18 hr in MY 33 and 7 hr in MY 34 are mainly due to the spread of observations in different latitudes and seasons. The diurnal variability of He shows a consistent formation of bulge on the nightside centered on ~2–6 hr in all the Martian years. The strength (density) and the local time extent of the bulge, however, decrease gradually with increase in altitude. This is particularly apparent in MY 35. The He densities inside the bulges are approximately an order of magnitude higher than those observed during daytime. Since CO_2 is the dominant neutral species in the Martian thermosphere and its variation from dayside-to-nightside is opposite to that of He (Bougher, Pawlowski, et al., 2015; Elrod et al., 2017), the He bulges can be better appreciated by normalizing the He densities with those of CO_2. As shown in the bottom panels of Figure 1, the He/CO_2 ratios show the formation of nightside He bulge at altitudes below 230 km. Above 230 km, existence of the bulge cannot be inferred due to the lower availability of CO_2 data. Note that Figure 1 gives a broad LST variability of He bulges but does not resolve their latitudinal or seasonal variability.

To further understand the seasonal, latitudinal and LST variability of the bulges, Figures 2a and 2b show the He/CO_2 ratios and He densities, respectively for an altitude of 200 km as a function of solar longitude (Ls). The top three panels in Figure 2 are color coded according to the season while the bottom panel is color coded according to LST. The seasons shown in Figure 2 correspond to ±45° centered on each Ls. Note that the gap from orbit #7093 to #8766 in Figure 2 is due to the exclusion of data during PEDE-2018. In Figure 2,

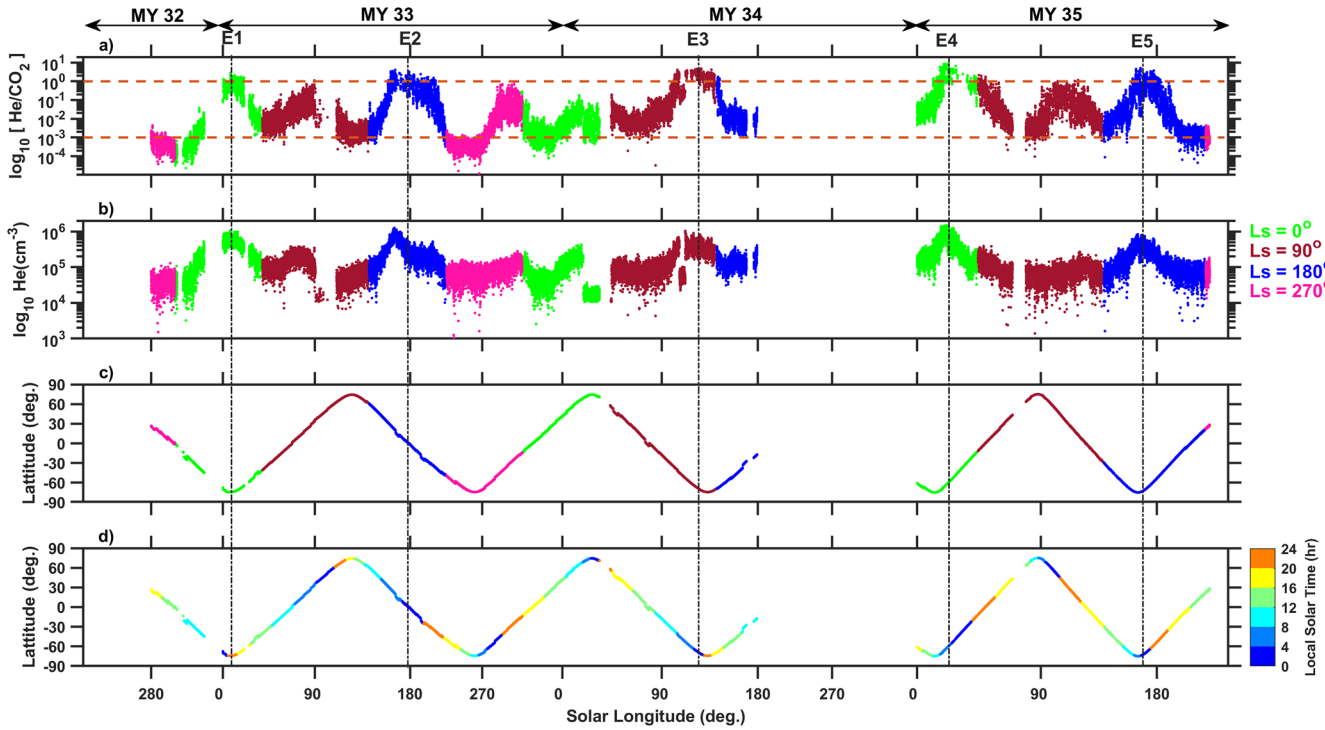

Figure 2. Temporal (as a function of Solar Longitude [Ls]) variation of (a) He/CO_2 ratios, (b) He density, and (c) MAVEN latitude, for 200 km and color coded according to the season. Each season covers ±45° Ls. Bottom panel is color coded according to the LST. In the top panel, horizontal red dashed lines are drawn to highlight the highest and lowest values of He/CO_2 ratios. Dominant He bulges are indicated by E1 to E5.

the existence of bulge can be better appreciated in He/CO_2 than in He alone. Irrespective of season and latitude, the He/CO_2 ratio increases during nighttime and decreases during daytime. The strongest bulges ($He/CO_2 > 1$), however, are clearly apparent in Ls = 0° (marked as E1 and E4), Ls = 90° (E3) and Ls = 180° (E2 and E5). Out of the five bulges, four bulges are observed in equinoxes (E1, E2, E4, and E5) and one bulge is observed in the southern winter. No considerable bulge is observed in Ls = 270°; however, due to limited data availability we cannot conclude on the formation/absence of the bulge in this season. By comparing with LST (Figure 2d), we can note that the bulges occur during nighttime, mostly in the early morning hours. Among the five bulges shown in Figure 2, four bulges (E1, E3, E4, and E5) occur in the southern high latitudes and one (E2) in the low-latitudes. There is some enhancement of He in the northern polar region at Ls = 0° (MY 34) but the same is not reflecting as bulge in He/CO_2 ratio. Overall, no appreciable bulge is observed in the northern high latitudes, partly due to the limited sampling of winter polar region near Ls ~ 270°.

LST-latitude variation of He densities for an altitude of 200 km are presented in Figure 3 for four seasons. Among the four seasons, data coverage is better for Ls = 90° (12.3%) and poor for Ls = 270° (4.7%). For Ls = 0°, the densities are near maximum (of all He densities in the season) in the southern polar nighttime (between 45° and 80°S; 3–8 LST). The densities are also relatively higher in the northern mid-latitudes during daytime (~30°–60°N; 10–13 LST), but are lowest in the northern polar nighttime (~70°N; 4–7 hr). In the northern summer solstice (Ls = 90°), the densities are near maximum in the southern high latitude nighttime (50°–80°S, 0–7 hr) and are minimum in the northern high-latitudes. For Ls = 180°, the densities are near maximum in the northern equatorial to mid-latitudes during nighttime (10°–30°N; 4–7 hr). The densities are also relatively higher in the southern high latitude nighttime (~60°–80°S; 1–8 hr). Much cannot be inferred from the density variation in Ls = 270°, except that the densities in the southern high latitudes are relatively smaller compared to those in Ls = 90°. Thus, in the northern summer solstice (Ls = 90°), the He bulge seems to form in the winter polar region (~50–80°S) whereas in equinoxes (Ls = 0° and = 180°) the bulges are not confined only to mid-latitudes but are extended to southern polar regions. Similar conclusions can be drawn about the bulges from He/CO_2 ratios (Figure 4) which show much better contrasts in

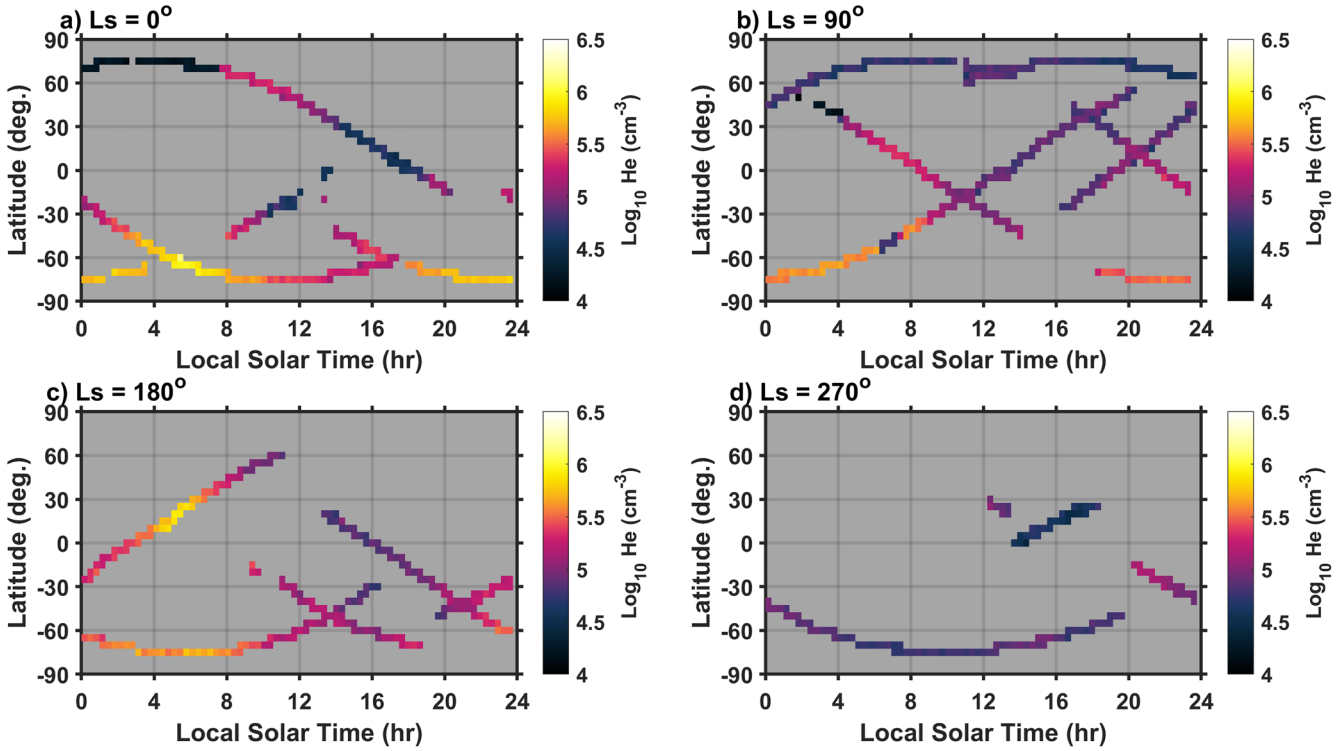

Figure 3. (a) Latitude versus local solar time variation of He density for panel (a–d) Ls 0°, 90°, 180°, and 270° as observed by NGIMS at 200 km. The data are averaged on a latitude and local time grid of 5° × 0.33 hr.

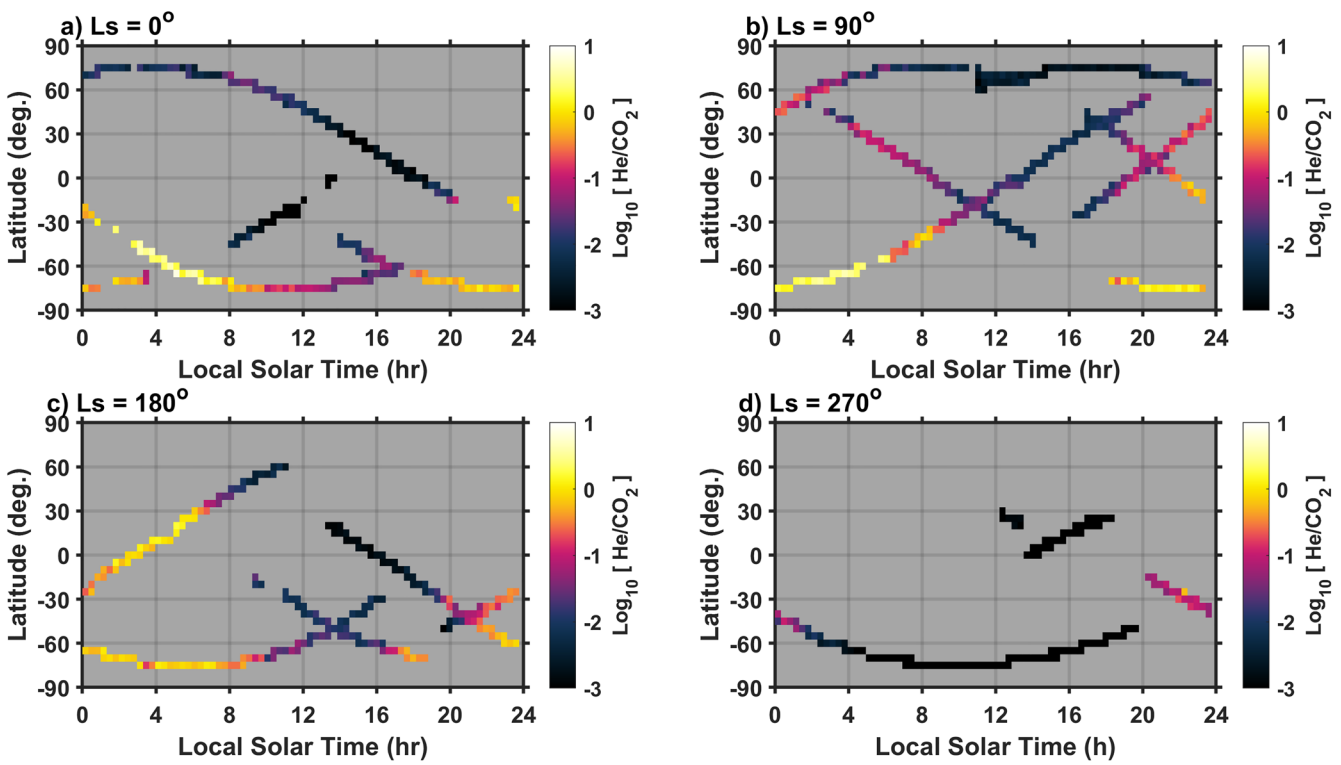

Figure 4. Similar to Figure 3, but for He/CO_2 ratios.

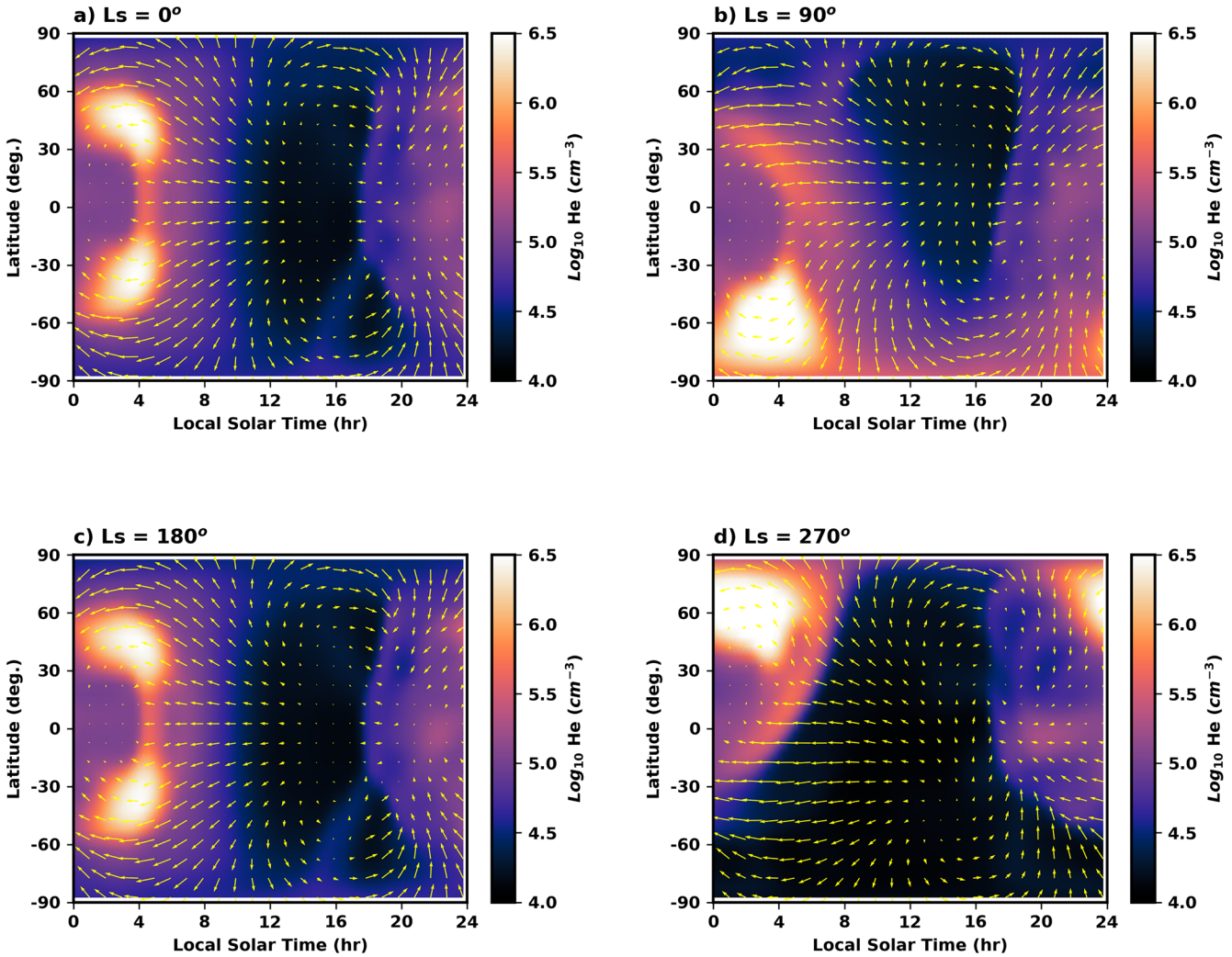

Figure 5. Similar to Figure 3, but the He densities shown are from M-GITM simulations for nominal dust conditions. The arrows show the modeled horizontal winds.

their variability. Note that the seasons considered here correspond to ±45° centered at each seasonal cardinal point (Ls = 0°, 90°, 180°, and 270°). Reducing the duration will not change the results (cf., Figure 2) but will lead to reduced data coverage in each season.

M-GITM predictions of the He bulges (color contours) and horizontal winds (yellow arrows) for an altitude of 200 km for the four seasons are shown in Figure 5. In the equinoxes (Ls = 0° and 180°), the bulges are observed between 1 and 5 hr at mid-latitudes (20–60°) with nearly equal strength on both the hemispheres. In solstices (Ls = 90° and 270°), the strongest bulges are observed in the winter polar nighttime. In Ls = 90°, there is a distinct (yet weak) second bulge between low- and mid-latitude regions in the northern hemisphere. Such a distinct secondary bulge, however, is not apparent at Ls = 270° but a continuous streak from the winter mid-latitudes to summer low-latitudes is observed. In addition, the winter bulge in solstices extends to pre-midnight hours and the extended portion of the bulges is stronger in Ls = 270° than in Ls = 90°. The modeled horizontal winds seem to converge in regions of the bulges. Comparing the modeled bulges in Figure 5 with the observed ones in Figure 4, we can note that the latitude and local time of predicted bulge differ from those of observed ones.

Comparison between the M-GITM predictions and the NGIMS observations is further carried out in Figure 6 which shows the ratios of the observed and modeled He densities (shown by color maps). In the latitudes and local times where the M-GITM predicts the formation of bulges in Ls = 0° and 90°, the observed

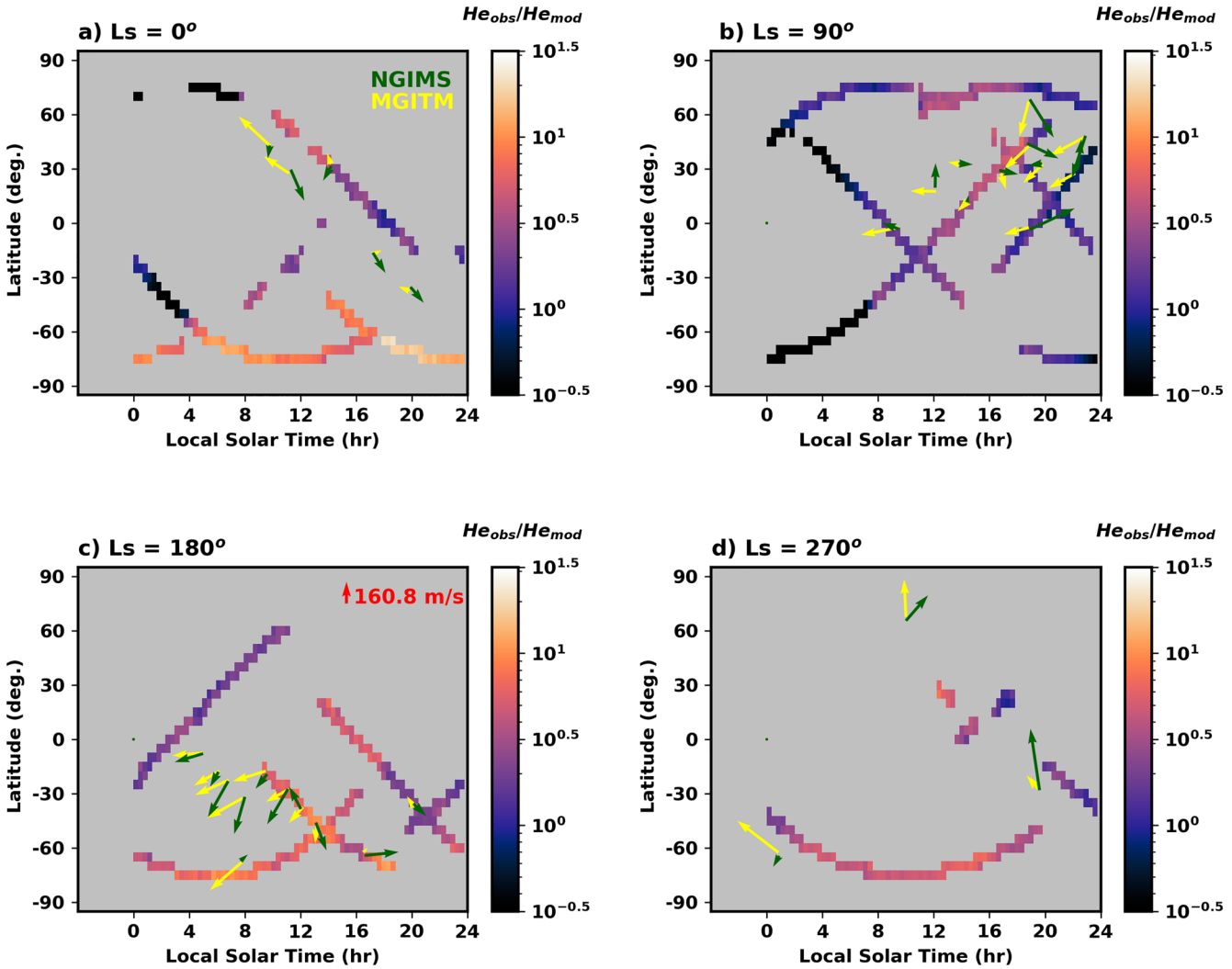

Figure 6. Similar to Figure 3 but shows the ratios of the observed and modeled He densities (shown by colorbar). The green and yellow arrows represent the winds observed by Neutral Gas and Ion Mass Spectrometer and modeled by M-GITM, respectively. Tails of the arrows show the location of the winds, length of the arrows show the magnitude (reference magnitude is shown by red arrow in panel c) and heads of the arrows point to the direction of the winds.

densities are slightly smaller than the modeled ones (deep blue colors). In the southern polar regions in equinoxes (Ls = 0° and 180°), however, the observed densities are 10–30 times higher than the modeled ones. Such underestimation by the model in the southern polar region (>60°S) is observed at all local times. The maximum discrepancies, however, are observed between 4–8 hr and 18–24 hr in Ls = 0°. Furthermore, the model underestimations extend to mid-latitudes during daytime which is observed in all seasons. In Ls = 270° also, the model slightly underestimates the observations in the southern polar regions.

To get a better understanding on the discrepancies in the location of the bulges in different seasons, the observed (green arrows) and modeled (yellow arrows) horizontal winds are also shown in Figure 6. The modeled winds are taken from those LST-latitude grids where the observations are available. The observed winds correspond to an altitude range of 200 ± 10 km whereas the modeled winds correspond to a constant altitude of 200 km. With the limited wind observations, we can note that in Ls = 0° the winds are mainly observed from equatorial and northern mid-latitudes whereas the bulges are observed in the southern hemisphere high latitudes. Thus, no firm conclusions regarding wind convergence in the southern polar night can be drawn. However, in Ls = 180°, the magnitudes of the observed and modeled winds match well but the observed winds, in general, point toward south whereas the modeled winds are more toward south–west. Thus, in Ls = 180° the observed winds point to the regions where observed densities exceed the

modeled ones. In Ls = 90°, the observed winds point in several different directions and hence it is difficult to draw any conclusions of their effect on the He density variations. Finally, only a few wind measurements are available in Ls = 270° and hence no conclusions are drawn.

4. Discussion

Characteristics of He bulges in the Martian thermosphere during nominal dust conditions are investigated using He densities and horizontal winds measured by the MAVEN NGIMS during 2015–2020 and 2016–2020, respectively and the modern M-GITM simulations. The following are the salient results of the present study.

1. In equinoxes, the He bulges are observed to extend from mid-latitudes into the southern polar regions (>60°S). Such an extension to polar latitudes is less obvious in the northern hemisphere, partly due to limited observations.
2. M-GITM predicts the formation of the bulges in the winter polar nightside latitudes (~45–80°) during solstices and in the mid-latitude (~20–60°) nightside in the equinoxes. The observed He densities in the southern polar regions (>60°S) in equinoxes are thus unexpected and are 10–30 × greater than the modeled ones.
3. The observed winds during the autumnal equinox (Ls = 180°) point to the direction of the observed He bulges whereas the modeled winds are slightly offset.
4. Winter polar bulge is clearly observed in the southern polar regions at Ls = 90° as predicted. Such a winter polar bulge, however, could not be observed in the northern polar regions at Ls = 270°, partly due to limited observations.

As predicted by models (Bougher, Pawlowski, et al., 2015) and previously reported from NGIMS observations (Elrod et al., 2017), He bulges are a persistent feature of the nightside Martian thermosphere. The densities inside the bulges are 1–2 orders higher than the dayside minimum densities. Similar to that observed at the Earth (Liu et al., 2014; Sutton et al., 2015), the He bulges on Mars are strongly seasonal dependent. Particularly, M-GITM predicts their formation at mid-latitudes (~20–60°) in equinoxes and at the winter poles (~45–80°) in solstices. For Earth, the local vertical advection and molecular diffusion are shown to be primary drivers of the bulge formation (Liu et al., 2014; Sutton et al., 2015). The seasonally varying horizontal winds contribute indirectly as their divergence on the dayside and convergence on the nightside drive the local vertical advection. Similar processes are likely to work on Mars as well (Elrod et al., 2017).

In the entire MAVEN data set, the northern winter pole was observed only twice: in MY 32 and MY 34. The initial observations of MAVEN (MY 32) were reported by Elrod et al. (2017) wherein their usage was cautioned due to possible instrumentation effects. As mentioned earlier, the MY 34 northern winter observations fall under PEDE-2018 which we did not include in the present study. As a result, we could not observe the He bulge in the northern winter polar region. The formation of the bulge in the northern winter pole reported by Elrod et al. (2017), however, is as predicted by the M-GITM simulations. In the present study, we report the first observations of the southern winter polar bulge which was observed by MAVEN in MY 34. These observations concur with the M-GITM predictions.

The most unexpected result of the present study is the formation of the bulges in the southern polar region (>60°S) in equinoxes. Even during daytime, the He densities at the southern polar region are greater than those at mid-latitudes. In equinoxes, the M-GITM predicts the formation of bulges at mid-latitudes (~20–60°) in both the northern and southern hemispheres. While there is also some enhancement in the mid-latitudes (30–60°), the most unexpected is the extension of the bulge to the southern polar region (60–80°S) which was clearly observed in the northern spring equinox (Ls = 0°). These bulges are in fact stronger than the one observed in the northern winter polar region by Elrod et al. (2017). The observed helium bulges at equinoxes thus extend beyond mid-latitudes and much closer to the southern pole than predicted. From the initial observations, Elrod et al. (2017) also noted these anomalous enhancements but was attributed to the instrumental effects. The present study clearly shows that the equinoxial He bulge extending to the southern pole is a persistent feature. Even the modern M-GITM simulations could not predict these anomalous equinox enhancements. This shows that the periodic solar insolation drivers of the Mars thermospheric circulation (e.g., solar heating changes on diurnal, seasonal, and solar cycle timescales) are not sufficient

to capture the high latitude convergence regions of global thermospheric winds implied by the helium distribution during equinox conditions. Therefore, other non-solar processes must be investigated. These processes include upward propagating gravity waves, which are thought to deposit their momentum and energy in the thermosphere and drive substantial changes in the otherwise solar driven upper atmosphere circulation (e.g., Medvedev & Yiğit, 2012). Addressing the coupling with the lower atmosphere via gravity wave momentum and energy deposition may be helpful to reproduce the observed southern polar helium bulge during equinoxes.

A comparison between the observed and modeled horizontal winds helps to some extent in understanding the formation of the equinoxial southern polar bulges. The convergent point of the modeled horizontal winds coincides with the locations of the modeled He bulges indicating that the horizontal winds lead to the local vertical advection. The magnitude and direction of the observed winds, however, deviates from the modeled winds. During the autumnal equinox (Ls = 180°) in particular, the observed winds point to the location of the southern polar bulge. This probably indicates that the actual location of the local vertical advection is in the southern polar region which is different from that predicted by M-GITM. To advance the present study, a larger wind database from NGIMS in the southern polar region is required, particularly during the equinoxes.

5. Conclusions

The present study reveals the detailed characteristics of the He bulges in the Martian upper atmosphere. In equinoxes, the bulges are expected to occur at mid-latitudes but are observed to extend into the southern polar region. While the observed winds seem to explain the anomalous occurrence of the bulge, there are some limitations. The winds in the northern spring equinox (Ls ~ 0°) are from northern mid-latitudes. It is not clear whether these winds maintain their southward direction at southern high and polar latitudes or not. However, measured winds near the southern spring equinox (Ls ~ 180°) seem to point to the general location of the helium bulge at high southern latitudes, whereas the M-GITM winds are slightly offset in direction. Thus, the results of the present study point to the need for more wind measurements, particularly from southern high and polar latitudes. This will help to improve the model and to elucidate the role of the horizontal winds in the formation of the bulge.

Data Availability Statement

The NGIMS (L2: V08_R01 plus L3:V06_R01) and EUVM (L3: V1_R01_2021015) data sets used in this study are publicly available at the MAVEN Science Data Center (https://lasp.colorado.edu/maven/sdc/public/pages/datasets/ngims.html for NGIMS and https://lasp.colorado.edu/maven/sdc/public/pages/datasets/euv.html for EUVM). M-GITM datacubes for the four-cardinal seasons during MY33 are archived on the University of Michigan Deep Blue Data repository (Bougher, 2021). The data corresponding to the figures in this work are publicly available on the Mendeley data repository (https://data.mendeley.com/datasets/jvzcpt65mh/1) (Gupta & Venkateswara Rao, 2021).

Acknowledgments
We are thankful to the anonymous reviewers for their helpful comments and suggestions. Research of M. K. Elrod and S. W. Bougher for this study is supported by the MAVEN project through Grant NNH10CC04C. The derived NGIMS products used in this study are based upon work supported by NASA under award number 80GSFC21M0002.

References

Benna, M., Bougher, S. W., Lee, Y., Roeten, K. J., Yiğit, E., Mahaffy, P. R., & Jakosky, B. M. (2019). Global circulation of Mars upper atmosphere. *Science*, *366*, 1363–1366. https://doi.org/10.1126/science.aax1553

Benna, M., & Elrod, M. (2019). *NGIMS PDS software interface specification MAVEN-NGIMS-SIS-0001, PDS atmospheres node*. Retrieved from http://atmos.pds.nasa.gov/data_and_services/atmospheresdata/MAVEN/ngims.html

Bhardwaj, A., Thampi, S. V., Das, T. P., Dhanya, M. B., Naik, N., Vajja, D. P., et al. (2016). On the evening time exosphere of Mars: Result from MENCA aboard Mars Orbiter Mission. *Geophysical Research Letters*, *43*, 1862–1867. https://doi.org/10.1002/2016GL067707

Bougher, S. (2021). *Mars thermospheric helium distributions: M-GITM simulated datasets for comparison to MAVEN/NGIMS measurements [data set]*. University of Michigan - Deep Blue Data. https://doi.org/10.7302/36zc-y350

Bougher, S. W., Blelly, P.-L., Combi, M., Fox, J. L., Mueller-Wodarg, I., Ridley, A., & Roble, R. G. (2008). Neutral upper atmosphere and ionosphere modeling. In A. F. Nagy, A. Balogh, T. E. Cravens, M. Mendillo, & I. Mueller-Wodarg (Eds.), *Comparative aeronomy*. Space Sciences Series of ISSI (Vol. 29, pp. 107–141). Springer. https://doi.org/10.1007/978-0-387-87825-6_4

Bougher, S. W., Cravens, T. E., Grebowksy, J., & Luhmann, J. (2015). The aeronomy of Mars: Characterization by MAVEN of the upper atmosphere reservoir that regulates volatile escape. *Space Science Reviews*, *195*, 423–456. https://doi.org/10.1007/s11214-014-0053-7

Bougher, S. W., Jakosky, B. M., Halekas, J., Grebowsky, J., Luhmann, J., Mahaffy, P., et al. (2015). Early MAVEN dip deep campaign reveals thermosphere and ionosphere variability. *Science*, *350*, aad0459. https://doi.org/10.1126/science.aad0459

Bougher, S. W., Pawlowski, D., Bell, J. M., Nelli, S., McDunn, T., Murphy, J. R., et al. (2015). Mars global ionosphere-thermosphere model: Solar cycle, seasonal, and diurnal variations of the Mars upper atmosphere. *Journal of Geophysical Research: Planets*, *120*, 311–342. https://doi.org/10.1002/2014JE004715

Bougher, S. W., Roeten, K. J., Olsen, K., Mahaffy, P. R., Benna, M., Elrod, M., et al. (2017). The structure and variability of Mars dayside thermosphere from MAVEN NGIMS and IUVS measurements: Seasonal and solar activity trends in scale heights and temperatures. *Journal of Geophysical Research: Space Physics*, *122*, 1296–1313. https://doi.org/10.1002/2016JA023454

Cageao, R. P., & Kerr, R. B. (1984). Global distribution of helium in the upper atmosphere during solar minimum. *Planetary and Space Science*, *32*(12), 1523–1529. https://doi.org/10.1016/0032-0633(84)90019-9

Elrod, M. K., Bougher, S., Bell, J., Mahaffy, P. R., Benna, M., Stone, S., et al. (2017). He bulge revealed: He and CO_2 diurnal and seasonal variations in the upper atmosphere of Mars as detected by MAVEN NGIMS. *Journal of Geophysical Research: Space Physics*, *122*, 2564–2573. https://doi.org/10.1002/2016JA023482

Elrod, M. K., Bougher, S. W., Roeten, K., Sharrar, R., & Murphy, J. (2020). Structural and compositional changes in the upper atmosphere related to the PEDE-2018 dust event on Mars as observed by MAVEN NGIMS. *Geophysical Research Letters*, *47*(4), e2019GL084378. https://doi.org/10.1029/2019GL084378

England, S. L., Liu, G., Yiğit, E., Mahaffy, P. R., Elrod, M., Benna, M., et al. (2017). MAVEN NGIMS observations of atmospheric gravity waves in the Martian thermosphere. *Journal of Geophysical Research: Space Physics*, *122*, 2310–2335. https://doi.org/10.1002/2016JA023475

Fritts, D. C., Wang, L., & Tolson, R. H. (2006). Mean and gravity wave structures and variability in the Mars upper atmosphere inferred from Mars Global Surveyor and Mars Odyssey aerobraking densities. *Journal of Geophysical Research*, *111*, A12304. https://doi.org/10.1029/2006JA011897

Gonzalez-Galindo, F., Chaufray, J.-Y., Lopez-Valverde, M. A., Gilli, G., Forget, F., Leblanc, F., et al. (2013). Three-dimensional Martian ionosphere model: The photochemical ionosphere below 180 km. *Journal of Geophysical Research*, *118*, 2105–2123. https://doi.org/10.1002/jgre.20150

González-Galindo, F., López-Valverde, M. A., Forget, F., García-Comas, M., Millour, E., & Montabone, L. (2015). Variability of the Martian thermosphere during eight Martian years as simulated by a ground-to-exosphere global circulation model. *Journal of Geophysical Research: Planets*, *120*, 2020–2035. https://doi.org/10.1002/2015JE004925

Gupta, N., & Venkateswara Rao, N. (2021). *Latitudinal and seasonal Asymmetries of the helium bulge in the Martian upper atmosphere* (version 1). Mendeley Data. https://doi.org/10.17632/jvzcpt65mh.1

Gupta, N., Venkateswara Rao, N., & Kadhane, U. R. (2019). Dawn-dusk asymmetries in the Martian upper atmosphere. *Journal of Geophysical Research: Planets*, *124*, 3219–3230. https://doi.org/10.1029/2019JE006151

Haberle, R. M., Joshi, M. M., Murphy, J. R., Barnes, J. R., Schofield, J. T., Wilson, G., et al. (1999). General circulation model simulations of the Mars Pathfinder atmospheric structure investigation/meteorology data. *Journal of Geophysical Research*, *104*, 8957–8974. https://doi.org/10.1029/1998JE900040

Hinson, D. P., Wilson, R. J., Smith, M. D., & Conrath, B. J. (2003). Stationary planetary waves in the atmosphere of Mars during southern winter. *Journal of Geophysical Research*, *108*(E1), 5004. https://doi.org/10.1029/2002JE001949

Jain, S. K., Bougher, S. W., Deighan, J., Schneider, N. M., Gonzalez-Galindo, F., Stewart, A. I. F., et al. (2020). Martian thermospheric warming associated with the Planet Encircling Dust Event of 2018. *Geophysical Research Letters*, *47*(3), E2019GL085302. https://doi.org/10.1029/2019GL085302

Johnson, F. S., & Gottlieb, B. (1970). Eddy mixing and circulation at ionospheric levels. *Planetary and Space Science*, *18*, 1707–1718. https://doi.org/10.1016/0032-0633(70)90004-8

Kasprzak, W. T. (1969). Evidence for a helium flux in the lower thermosphere. *Journal of Geophysical Research*, *74*, 894–896. https://doi.org/10.1029/JA074I003P00894

Kasprzak, W. T., Neiman, H. B., Hedin, A. E., Bougher, S. W., & Hunten, D. M. (1993). Neutral composition measurements by the pioneer Venus neutral mass spectrometer during orbiter re-entry. *Geophysical Research Letters*, *20*, 2747–2750. https://doi.org/10.1029/93GL02241

Keating, G., & Prior, E. (1968). The winter helium bulge. *Space Research*, *8*, 982.

Krasnopolsky, V. A., Bowyer, S., Chakrabarti, S., Gladstone, G. R., & McDonald, J. S. (1994). First measurement of helium on Mars: Implications for the problem of radiogenic gases on the terrestrial planets. *Icarus*, *109*, 337–351. https://doi.org/10.1006/icar.1994.1098

Krasnopolsky, V. A., & Gladstone, G. R. (2005). Helium on Mars and Venus: EUVE observations and modeling. *Icarus*, *176*, 395–407. https://doi.org/10.1016/j.icarus.2005.02.005

Kuroda, T., Medvedev, A. S., & Yiğit, E. (2020). Gravity wave activity in the atmosphere of Mars during the 2018 global dust storm: Simulations with a high-resolution model. *Journal of Geophysical Research: Planets*, *125*(11), E2020JE006556. https://doi.org/10.1029/2020JE006556a

Leblanc, F., Benna, M., Chaufray, J. Y., Martinez, A., Lillis, R., Curry, S., et al. (2019). First in situ evidence of Mars nonthermal exosphere. *Geophysical Research Letters*, *46*, 4144–4150. https://doi.org/10.1029/2019GL082192

Lee, C., Lawson, W. G., Richardson, M. I., Heavens, N. G., Kleinböhl, A., Banfield, D., et al. (2009). Thermal tides in the Martian middle atmosphere as seen by the Mars Climate Sounder. *Journal of Geophysical Research*, *114*, E03005. https://doi.org/10.1029/2008JE003285

Leelavathi, V., Venkateswara Rao, N., & Rao, S. V. B. (2020). Inter-annual variability of atmospheric gravity waves in the Martian thermosphere: Effects of the 2018 planet-encircling dust event. *Journal of Geophysical Research: Planets*, *125*, E2020JE006649. https://doi.org/10.1029/2020je006649

Liu, G., England, S., Lillis, R. J., Mahaffy, P. R., Elrod, M., Benna, M., & Jakosky, B. (2017). Longitudinal structures in Mars' upper atmosphere as observed by MAVEN/NGIMS. *Journal of Geophysical Research: Space Physics*, *122*, 1258–1268. https://doi.org/10.1002/2016JA023455

Liu, G., England, S. L., Lillis, R. J., Withers, P., Mahaffy, P. R., Rowland, D. E., et al. (2018). Thermospheric expansion associated with dust increase in the lower atmosphere on Mars observed by MAVEN/NGIMS. *Geophysical Research Letters*, *45*, 2901–2910. https://doi.org/10.1002/2018GL077525

Liu, X., Wang, W., Thayer, J. P., Burns, A., Sutton, E., Solomon, S. C., et al. (2014). The winter helium bulge revisited. *Geophysical Research Letters*, *41*, 6603–6609. https://doi.org/10.1002/2014GL061471

Mahaffy, P. R., Benna, M., King, T., Harpold, D. N., Arvey, R., Barciniak, M., et al. (2014). The neutral gas and ion mass spectrometer on the Mars atmosphere and volatile evolution mission. *Space Science Reviews*, *195*, 49–73. https://doi.org/10.1007/s11214-014-0091-1

Mahaffy, P. R., Benna, M., Elrod, M., Yelle, R. V., Bougher, S. W., Stone, S. W., & Jakosky, B. M. (2015). Structure and composition of the neutral upper atmosphere of Mars from the MAVEN NGIMS investigation. *Geophysical Research Letters*, *42*, 8951–8957. https://doi.org/10.1002/2015GL065329

Mauersberger, K., Potter, W., & Kayser, D. (1976). A direct measurement of the winter helium bulge. *Geophysical Research Letters*, *3*, 269–271. https://doi.org/10.1029/gl003i005p00269

Medvedev, A. S., & Yiğit, E. (2012). Thermal effects of internal gravity waves in the Martian upper atmosphere. *Geophysical Research Letters*, *39*, L05201. https://doi.org/10.1029/2012GL050852

Montabone, L., Forget, F., Millour, E., Wilson, R. J., Lewis, S. R., Cantor, B., et al. (2015). Eight-year climatology of dust optical depth on Mars. *Icarus*, *251*, 65–95. https://doi.org/10.1016/j.icarus.2014.12.034

Moudden, Y., & Forbes, J. (2010). A new interpretation of Mars aerobraking variability: Planetary wave-tide interactions. *Journal of Geophysical Research*, *115*, E09005. https://doi.org/10.1029/2009JE003542

Niemann, H. B., Kasprzak, W. T., Hedin, A. E., Hunten, D. M., & Spencer, N. W. (1980). Mass spectrometric measurements of the neutral gas composition of the thermosphere and exosphere of Venus. *Journal of Geophysical Research*, *85*, 7817–7827. https://doi.org/10.1029/JA085iA13p07817

Pilinski, M., Bougher, S. W., Greer, K., Thiemann, E., Andersson, L., Benna, M., & Elrod, M. (2018). First evidence of persistent night-time temperature structures in the neutral thermosphere of Mars. *Geophysical Research Letters*, *45*, 8819–8825. https://doi.org/10.1029/2018GL078761

Reber, C., Cooley, J., & Harpold, D. (1968). Upper atmosphere hydrogen and helium measurements from the Explorer 32 satellite. *Space Research*, *8*, 993.

Reber, C. A., & Hays, P. B. (1973). Thermospheric wind effects on the distribution of helium and argon in the Earth's upper atmosphere. *Journal of Geophysical Research*, *78*, 2977–2991. https://doi.org/10.1029/JA078i016p02977

Roeten, K. J., Bougher, S. W., Benna, M., Mahaffy, P. R., Lee, Y., Pawlowski, D., et al. (2019). MAVEN/NGIMS thermospheric neutral wind observations: Interpretation using the M-GITM general circulation model. *Journal of Geophysical Research: Planets*, *124*, 3283–3303. https://doi.org/10.1029/2019je005957

Smith, M. D. (2004). Interannual variability in TES atmospheric observations of Mars during 1999–2003. *Icarus*, *167*(1), 148–165. https://doi.org/10.1016/j.icarus.2003.09.010

Smith, M. D. (2009). THEMIS observations of Mars aerosol optical depth from 2002–2008. *Icarus*, *202*(2), 444–452. https://doi.org/10.1016/j.icarus.2009.03.027

Stone, S. W., Yelle, R. V., Benna, M., Elrod, M. K., & Mahaffy, P. R. (2018). Thermal structure of the Martian upper atmosphere from MAVEN NGIMS. *Journal of Geophysical Research: Planets*, *123*, 2842–2867. https://doi.org/10.1029/2018JE005559

Sutton, E. K., Thayer, J. P., Wang, W., Solomon, S. C., Liu, X., & Foster, B. T. (2015). A self-consistent model of helium in the thermosphere. *Journal of Geophysical Research: Space Physics*, *120*, 6884–6900. https://doi.org/10.1002/2015JA021223

Terada, N., Leblanc, F., Nakagawa, H., Medvedev, A. S., Yiğit, E., Kuroda, T., et al. (2017). Global distribution and parameter dependences of gravity wave activity in the Martian upper thermosphere derived from MAVEN/NGIMS observations. *Journal of Geophysical Research: Space Physics*, *122*, 2374–2397. https://doi.org/10.1002/2016JA023476

Thayer, J., Liu, X., Lei, J., Pilinski, M., & Burns, A. (2012). The impact of helium on thermosphere mass density response to geomagnetic activity during the recent solar minimum. *Journal of Geophysical Research*, *117*, A07315. https://doi.org/10.1029/2012JA017832

Thiemann, E. M. B., Andersson, L., Lillis, R., Withers, P., Xu, S., Elrod, M., et al. (2018). The Mars topside ionosphere response to the X8.2 solar flare of 10 September 2017. *Geophysical Research Letters*, *45*, 8005–8013. https://doi.org/10.1029/2018gl077730

Thiemann, E. M. B., Chamberlin, P. C., Eparvier, F., Woods, T., Bougher, S. W., Jakosky, B. M., & Templeman, B. (2017). The MAVEN EUVM spectral irradiance model for solar variability at Mars: Algorithms and results. *Journal of Geophysical Research: Space Physics*, *122*, 2748–2767. https://doi.org/10.1002/2016JA023512

Thiemann, E. M. B., Eparvier, F. G., Andersson, L. A., Fowler, C. M., Peterson, W. K., Mahaffy, P. R., et al. (2015). Neutral density response to solar flares at Mars. *Geophysical Research Letters*, *42*, 8986–8992. https://doi.org/10.1002/2015GL066334

Venkateswara Rao, N., Gupta, N., & Kadhane, U. R. (2020). Enhanced densities in the Martian thermosphere associated with the 2018 planet-encircling dust event: Results from MENCA/MOM and NGIMS/MAVEN. *Journal of Geophysical Research: Planets*, *125*, e2020JE006430. https://doi.org/10.1029/2020je006430

Williamson, H. N., Johnson, R. E., Leclercq, L., & Elrod, M. K. (2019). Large amplitude perturbations in the Martian exosphere seen in MAVEN NGIMS data. *Icarus*, *331*, 110–115. https://doi.org/10.1016/j.icarus.2019.05.020

Wilson, R. J. (2002). Evidence for nonmigrating thermal tides in the Mars upper atmosphere from the Mars global surveyor accelerometer experiment. *Geophysical Research Letters*, *29*(7), 1120. https://doi.org/10.1029/2001GL013975

Zurek, R. W., Tolson, R. A., Bougher, S. W., Lugo, R. A., Baird, D. T., Bell, J. M., & Jakosky, B. M. (2017). Mars thermosphere as seen in MAVEN accelerometer data. *Journal of Geophysical Research: Space Physics*, *122*(3), 3798–3814. https://doi.org/10.1002/2016ja023641